Drug powders with tunable wettability by atomic and molecular layer deposition
From highly hydrophilic to superhydrophobic

Zara, Damiano La; Zhang, Fuweng; Sun, Feilong; Bailey, Maximilian R.; Quayle, Michael J.; Petersson, Gunilla; Folestad, Staffan; van Ommen, J. Ruud

DOI
10.1016/j.apmt.2021.100945

Publication date
2021

Document Version
Final published version

Published in
Applied Materials Today

Citation (APA)
Zara, D. L., Zhang, F., Sun, F., Bailey, M. R., Quayle, M. J., Petersson, G., Folestad, S., & van Ommen, J. R. (2021). Drug powders with tunable wettability by atomic and molecular layer deposition: From highly hydrophilic to superhydrophobic. *Applied Materials Today*, *22*, Article 100945. https://doi.org/10.1016/j.apmt.2021.100945

Applied Materials Today 22 (2021) 100945

Contents lists available at ScienceDirect

Applied Materials Today

journal homepage: www.elsevier.com/locate/apmt

Drug powders with tunable wettability by atomic and molecular layer deposition: From highly hydrophilic to superhydrophobic

Damiano La Zara[a,1], Fuweng Zhang[a,1,*], Feilong Sun[a], Maximilian R. Bailey[a,b], Michael J. Quayle[c], Gunilla Petersson[d], Staffan Folestad[d], J. Ruud van Ommen[a]

[a] Department of Chemical Engineering, Delft University of Technology, Van der Maasweg 9, Delft 2629HZ, The Netherlands
[b] Department of Materials, Laboratory for Soft Materials and Interfaces, ETH Zürich, Vladimir-Prelog Weg 5, Zürich 8093, Switzerland
[c] New Modalities and Parenteral Development, Pharmaceutical Technology & Development, Operations, AstraZeneca, Gothenburg, Sweden
[d] Innovation Strategy and External Liaison, Pharmaceutical Technology & Development, Operations, AstraZeneca, Gothenburg, Sweden

ARTICLE INFO

Article history:
Received 21 September 2020
Revised 11 January 2021
Accepted 13 January 2021

Keywords:
Atomic layer deposition
Molecular layer deposition
Wetting
Pharmaceutical powder
Budesonide
Hydrophilic/hydrophobic

ABSTRACT

The wettability of pharmaceuticals is a key physical property which influences their dissolution rate, dispersibility, flowability and solid-state stability. Here, we provide a platform of surface nanoengineering methods capable of tuning the wettability of drug powders from high hydrophilicity to superhydrophobicity with drug loadings up to 95–99%. Specifically, we functionalize gram-scale micronized budesonide, a commercial active pharmaceutical ingredient for respiratory diseases, in a vibrated fluidized bed reactor with inorganic Al_2O_3, TiO_2 and SiO_2 by atomic layer deposition (ALD), organic poly(ethylene terephthalate) (PET) by molecular layer deposition (MLD) and inorganic/organic titanicone by hybrid ALD/MLD. Transmission electron microscopy shows the formation of smooth and uniform films for each deposition process without significantly affecting the surface morphology of the budesonide particles. Crucially, the deposition processes do not alter the solid-state structure and cytocompatibility of budesonide. The ceramic ALD films are able to convert the originally hydrophobic budesonide into highly hydrophilic powders with water contact angles (WCAs) of ~10° within a few seconds. The purely organic PET films grown via MLD deliver superhydrophobic powders with a WCA of 145–150°. In contrast, the titanicone hybrid ALD/MLD films lead to mild hydrophilicity with WCAs ranging from ~80° to ~60°. Modifying the wetting properties of inhaled drug powders such as budesonide is relevant to improve bioavailability, enhance the dispersion of formulations in suspension-based inhalers or prevent moisture interactions in dry powder inhalers. Moreover, by tuning the surface chemical composition at the atomic or molecular level, particle ALD, MLD and hybrid ALD/MLD enable control over powder wettability for several pharmaceutical dosage forms with applications in oral, orally inhaled and parenteral delivery.

1. Introduction

Surface properties of pharmaceutical particles play an important role in both the formulation, storage and performance of dosage forms. In particular, wettability is one of the most crucial surface characteristics, as it affects several factors: (i) dissolution rate of solid particles, as wetting is a precursor to dissolution [1–3]; (ii) disintegration of tablets [4–6]; (iii) dispersibility in liquid-based dosage forms [7]; (iv) flowability of powders during both the manufacturing process [8] and drug delivery such as inhalation [9,10]; and (v) solid-state stability in spray-dried materials [11,12]. Improved water wettability of pharmaceutical powders facilitates their dispersibility, which is their ability to break down into particles, when in contact with body fluids, thus easing deaggregation and wetting steps in the dissolution process. In suspension-based inhaled formulations, which necessitate the use of organic solvents, surfactants and lipids as excipients, the drug needs to be properly dispersed and form a stable suspension to ensure precise filling during manufacturing and accurate dosing during inhalation [13,14]. On the other hand, in amorphous solid inhalable dispersions, which are characterized by physical and chemical instability and moisture sensitivity, protection against moisture ingress is crucial [15]. Moreover, for inhaled hygroscopic drugs, their adhesive

* Corresponding author.
E-mail addresses: F.Zhang-9@tudelft.nl (F. Zhang), J.R.vanOmmen@tudelft.nl (J.R. van Ommen).
[1] These authors contributed equally to this work.

https://doi.org/10.1016/j.apmt.2021.100945

and cohesive properties can be altered and sometimes irreversible aggregation can occur due to the significant moisture uptake and formation of liquid bridges, which negatively affect aerosolization and lung deposition [16]. Therefore, tuning the wetting of drug powders based on the desired formulation design is highly desirable.

Several approaches to modify the wettability of pharmaceutical powders have been investigated to date [17–22]. Liquid-based coating methods, despite their simplicity, present a number of drawbacks such as complex and time-consuming separation and drying steps, high energy consumption due to the evaporation of organic and aqueous solvents involved in the process, and environmental pollution arising from highly volatile organic solvents [23–25]. On the other hand, conventional dry coating methods, while avoiding the use of solvents and thus reducing both processing time and contamination, still require a large amount of guest material to achieve the desired wetting properties [18,26]. Physical and chemical vapor deposition (PVD and CVD) have the potential to minimize the amount of coating material, and thus increase the final drug loading. In PVD techniques, the coating material is evaporated by sublimation in high vacuum environment using high temperature or plasma processes, and then transported to the substrate where it undergoes condensation to form a thin film [27]. In CVD, typically two gaseous precursors are introduced simultaneously in the reaction chamber, where they react in the gas phase to produce the material to be deposited as a thin film on the substrate surface [28]. However, both PVD and CVD are not well suited to uniformly and conformally coat complex three-dimensional structures such as pharmaceutical particles with films in the low nanometer range [29,30]. As a result, the control over surface composition and morphology is often compromised.

Atomic layer deposition (ALD), molecular layer deposition (MLD) and their combination hybrid ALD/MLD are vapor deposition techniques based on sequential self-limiting reactions of a precursor and a co-reactant separated by purge steps in a cyclical manner [31,32]. In doing so, the thickness of the films is controlled at the atomic or molecular level. ALD has therefore been utilised to modify the wetting properties of mainly polymeric substrates [33–37]. A number of studies have proven the intrinsically hydrophilic nature of metal oxides grown by ALD, such as Al_2O_3 and TiO_2 [33,37–41]. However, a few ALD cycles can also turn naturally hydrophilic cellulosic materials hydrophobic. This is attributed to nanoscale surface roughness which is prevalent during the early growth stages of the film, as well as to the adsorption of adventitious carbon [36,42,43]. Furthermore, ALD-grown semiconductive oxides such as ZnO and TiO_2 have been shown to reversibly change their contact angle upon exposure to ultraviolet light [44–46]. On the other hand, the use of MLD has been demonstrated to enhance the dispersibility of particles in organic media [47–49]. The organic polymer films, in fact, make the particles preferentially disperse within the organic phase, which indicates their oleophilic nature after the MLD functionalization. In particular, suspensions of polyurea-coated carbon nanotubes in organic solvents could remain stable for weeks under ambient conditions [47], whereas poly(ethylene terephthalate)-coated Sn nanofluids showed good stability even after treatment for 24 h at 140 °C [49]. Dispersing particles in organic media is relevant for pharmaceutical applications, such as Pickering emulsions [50]and solid dispersion systems [51]. However, neither MLD nor hybrid ALD/MLD have yet been applied to tailor the wettability of drug particles. Moreover, a comprehensive investigation on the potential of ALD, MLD and hybrid ALD/MLD to achieve the full range of wetting properties for particulate materials is still lacking.

Here, we report the deposition of nanoscale inorganic, organic and inorganic/organic films by ALD, MLD and hybrid ALD/MLD, respectively, to tune the wettability of micronized budesonide powders, a potent anti-inflammatory corticosteroid for respiratory diseases. Al_2O_3, TiO_2 and SiO_2 were grown as inorganic ceramic materials, poly(ethylene terephthalate) as organic, and titanicone as inorganic/organic. To reduce the influence of surface roughness on the wetting performance and minimize the amount of coating material, sufficiently thick films were synthesized by carrying out the deposition processes for 10 and 50 cycles for Al_2O_3, TiO_2 and titanicone, 50 cycles for PET and 100 cycles for SiO_2. The film morphology and thickness were examined by transmission electron microscopy (TEM). The solid-state stability of the budesonide particles after ALD and MLD was verified by X-ray powder diffraction (XRPD). The cytocompatibility of ALD-coated budesonide was assessed by cell viability tests using human epithelial alveolar A549 cells. The wetting of uncoated and coated budesonide was quantified by water contact angle measurements on the powder layer using the sessile drop method. The dispersibility in water was further investigated by zeta potential analysis. Finally, particle size distributions of uncoated and ALD-coated budesonide in water were measured to estimate the suspended particle and agglomerate size.

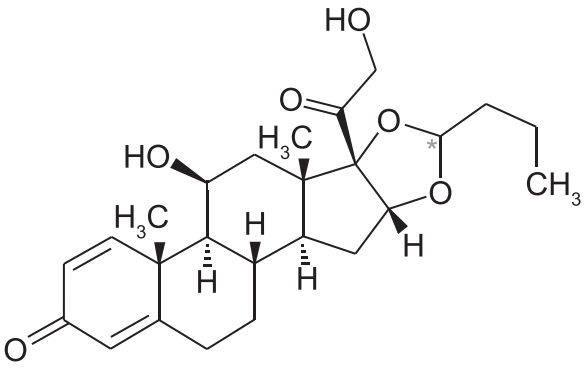

Fig. 1. Chemical structure of budesonide.

2. Experimental

2.1. Materials

Micronized budesonide particles with a particle size distribution ranging from 0.1 to 10 μm and a specific surface area of ~5.6 m^2/g were received from AstraZeneca and used as a substrate for the deposition [40]. The chemical structure of budesonide is depicted in Fig. 1. The ALD precursors, trimethylaluminum (TMA), titanium tetrachloride ($TiCl_4$) and silicon tetrachloride ($SiCl_4$), were purchased from Nouryon, Strem Chemicals and Alfa Aesar, respectively, and used as received. Ozone was employed as a co-reactant with TMA, whereas demineralized water as a co-reactant with $TiCl_4$ and $SiCl_4$. The MLD precursors, terephthaloyl chloride (TC) and ethylene glycol (EG), were obtained from Sigma-Aldrich and used as received. Each precursor was stored in a stainless steel bubbler under an inert atmosphere.

2.2. ALD, MLD and Hybrid ALD/MLD Experiments

ALD, MLD and hybrid ALD/MLD experiments were carried out in a vibrated fluidized bed reactor operating at atmospheric pressure, as described elsewhere [40,41,48]. The ALD precursors, i.e., TMA, $TiCl_4$ and $SiCl_4$, and co-reactants, i.e., O_3 and H_2O, were kept at room temperature, whereas the MLD precursors, i.e., TC and EG, were heated to 100 °C (see Table S1). N_2 (99.999 v/v%) was used as both carrier and purging gas. The lines were kept at 30 °C above the bubblers' temperature to avoid undesired condensation and under-delivery of precursors. The reactor was operated at a temperature of 40 °C for the ALD experiments, 150 °C for the MLD

experiment and 120 °C for the hybrid ALD/MLD experiment (see Table S1). For the ALD and MLD experiments, budesonide powder batches of 5 g were loaded into the reactor, whereas 8 g were used in the hybrid ALD/MLD experiment. Optimized gas flows of 1 NL/min, corresponding to 3.4 cm/s at room temperature, for 5 g of budesonide and 2 NL/min, corresponding to 6.7 cm/s at room temperature, for 8 g of budesonide were employed to deliver the precursors to the reactor and sufficiently mix the powder with the assistance of mechanical vibration. ALD of Al_2O_3 and TiO_2 and hybrid ALD/MLD of titanicone were run for 10 and 50 cycles, MLD of PET for 50 cycles, whereas ALD of SiO_2 for 100 cycles. The precursors and their exposure times in each deposition process are reported in Table S1.

2.3. Material Characterization

The presence and morphology of the ALD, MLD and hybrid ALD/MLD films on the budesonide particles was assessed by transmission electron microscopy (TEM). The samples were prepared by directly dispersing the powders on copper TEM grids of 3.05 mm in diameter. TEM images of several particles on the grid were taken using a JEOL JEM-1400 electron microscope operating at 120 kV. The thickness of the Al_2O_3, TiO_2, SiO_2, PET and titanicone films was evaluated with the ImageJ software. For each sample, the film thickness of more than 10 particle agglomerates was measured at various locations and averaged. To quantify the inorganic content in the ALD-coated and hybrid-coated budesonide, elemental analysis was carried out by inductively coupled plasma optical emission spectrometry (ICP–OES). Approximately 30 mg of powder was destructed in 4.5 ml of 30% HCl, 1.5 ml of 65% HNO_3 and 1 ml of 40% HF using the microwave Multiwave PRO. The destruction time in the microwave was 60 min at maximum power. After destruction, the samples were diluted to 50 ml with Milli-Q water and analysed with a PerkinElmer Optima 5300 DV optical emission spectrometer. The crystal structure of uncoated and ALD-coated budesonide was examined by X-ray powder diffraction (XRPD). The diffractograms were obtained by a Bruker AXS D8 Discover diffractometer with Co K_α radiation. The angle 2θ was scanned from 5° to 50° with steps of 0.02°.

2.4. Cell Viability Analysis

The cell viability analysis of uncoated and ALD-coated budesonide was carried out with the human epithelial alveolar A549 cell line. A549 cells were purchased from the American Type Culture Collection (ATCC). The cells were cultured in 75 cm^2 culture flasks (Corning Inc. Life Sciences) using 15 mL Dulbeccos modified Eagles medium (DMEM) in an incubator at 37 °C in an atmosphere of 5% CO_2 and 95% relative humidity. The medium was supplemented with 10% heat inactivated fetal bovine serum (FBS, Sigma-Aldrich) and antimycotic solution (1% v/v). The growth medium was changed every other day until the time of use. A549 cells were seeded on 96 wellplates at a density of 1×10^4 cells per well and cultured overnight. The media was aspirated from all the wells, and the cells were then treated with a concentration of 100 µM of budesonide formulation which was dispersed and diluted in 100 µL cell culture media for each well. After incubation for 24 h, cell viability was evaluated by adding 10 µL CCK-8 reagent (Sigma-Aldrich) to each well and incubated for an additional 2 h at 37°C under the condition of 5% CO_2 and 95% relative humidity. The optical density was measured by using a Microplate Reader (Multiskan FC, Thermo Scientific) at 450 nm with a reference absorbance at 620 nm, according to the manufacturer's protocol.

2.5. Water Contact Angle

The water contact angle (WCA) was measured by a Drop Shape Analyzer (DSA30, KRUSS GmbH). In each measurement, a deionized water droplet with a volume of 11.5 µL was generated by a syringe and gently dripped on the surface of the budesonide powder film (see Figure S1). The powder film was prepared by using a spatula and leveler to ensure a smooth surface formed when measuring the tangent angle at the contact point of the three phases [52–54]. The spreading process of the water droplet into the powder surface was recorded by the CCD camera for 5 min at a temperature of 18 °C. The contact angles were then directly measured from the captured drop profiles using the drop-shape analysis program, consisting of different sessile drop fitting methods. The measured contact angle is then plotted as a function of time after the water drop is placed on the powder surface. For each sample, the water contact angle measuremens were repeated 10 times and the resulting values were then averaged to compare the material wettability. In case of good wettability, the water droplet would fully spread into the powder bed, acting as a binder and leading to the formation of strongly bound, wet granules. The ALD-coated powder films were thus dried overnight at 40 °C, gently excavated and photographed to observe the resulting granule structure.

2.6. Dispersibility in Water

Zeta potential measurements of 1 mg/mL particle suspensions in Milli-Q ultrapure water were recorded using a Zetasizer Nano ZS (Malvern Instruments) and the inbuilt software. Samples were calibrated for 5 minutes, and values were averaged over 4 measurements, with 40 runs per measurement. Suspensions of 1 mg/mL were also prepared by placing 10 mg of uncoated and coated budesonide powders in 10 mL of distilled water. The suspensions were then agitated with a RO 15 power IKAMAG(R) magnetic stirring plate for 1 min to properly disperse the powder, and photographed. The particle size distributions of uncoated and ALD-coated budesonide in water were measured via laser diffraction with a Malvern Mastersizer 3000 in combination with the Hydro MV with a volume of 120 mL. This configuration has a measuring range from 0.01 µm up to 2100 µm. The optical model of Fraunhofer, which does not require knowledge of the optical properties of the sample and assumes the particles to be opaque, was applied.

3. Results and discussion

3.1. Deposition of inorganic and organic nanoscale films

ALD, MLD and hybrid ALD/MLD enable the fabrication of uniform and conformal nanoscale films on virtually any substrate. In particular, inorganic films can be obtained by ALD, purely organic films by MLD and hybrid inorganic/organic films by hybrid ALD/MLD. Inorganic films, namely Al_2O_3, TiO_2 and SiO_2, were deposited on micronized budesonide particles via TMA/O_3, $TiCl_4$/H_2O and $SiCl_4$/H_2O ALD, respectively. Comparable loadings of 6.1, 4.5 and 6.8 wt. %, corresponding to budesonide loadings of 93.9, 95.5 and 93.2 wt. %, were found for Al_2O_3 and TiO_2 after 10 cycles, and SiO_2 after 100 cycles, respectively (see Tables S2 to S4 and Equation (S1)). TEM observations of Al_2O_3-coated budesonide suggested the formation of 20 and 50 nm thick films on average after 10 and 50 cycles, respectively (see Figs. 2, S2). The thicknesses observed under TEM were then compared to the theoretical thicknesses resulting from the Al_2O_3 wt. %, measured by ICP-OES, according to Equation (S3), which applies to core-shell particles with an external shell. A large discrepancy is found between the thicknesses calculated from the Al_2O_3 wt. % and the thicknesses observed under TEM (see Figure S3), which indicates that Al_2O_3 does

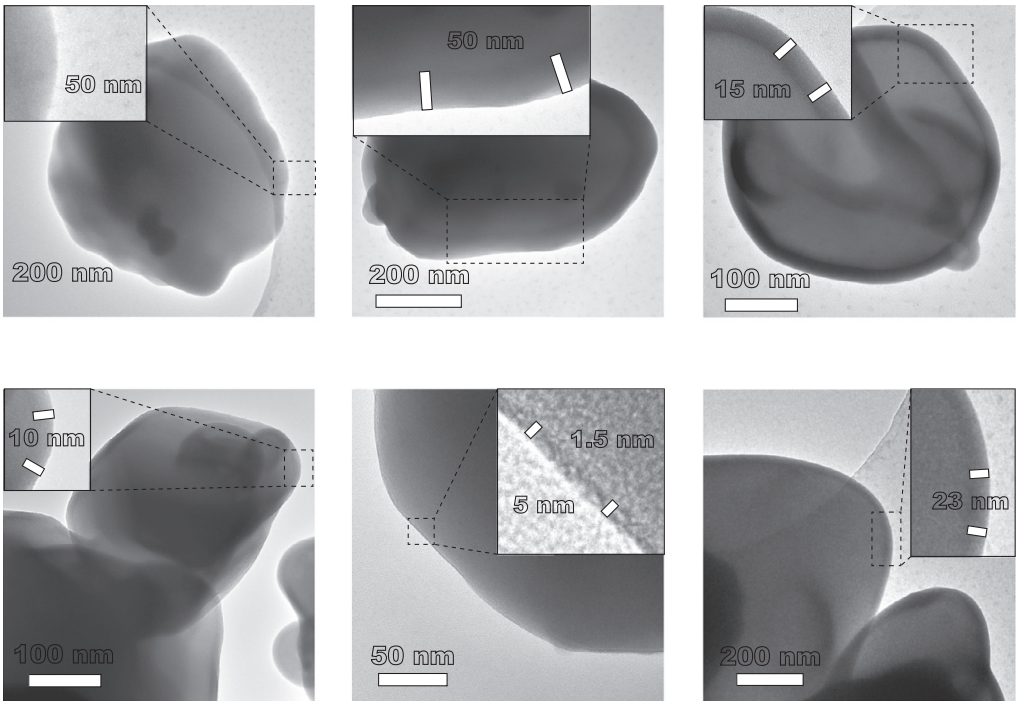

Fig. 2. TEM images of budesonide particles, uncoated and coated by SiO_2, Al_2O_3 and TiO_2 films via ALD, by poly(ethylene) terephthalate films via MLD and by titanicone films via $TiCl_4$/EG hybrid ALD/MLD. The deposition processes of Al_2O_3, TiO_2, PET and titanicone were run for 50 cycles, wheres that of SiO_2 for 100 cycles. The details of the experimental conditions are reported in Table S1. The film thicknesses were measured by ImageJ.

not mainly grow at the surface and instead infiltrates into budesonide. TMA, in fact, does not readily react on the surface due to the low number of OH surface groups and instead mostly diffuses into the budesonide core, leading to sub-surface growth and the formation of highly thick films consisting of an Al_2O_3-budesonide mixture. Despite the inherent lack of conformality, i.e., unequal thickness across different particles, smooth films were still obtained. This penetration phenomenon is widely reported in ALD on biomaterials and polymers, which are permeable to aggressive and highly reactive metal precursors such as TMA that can exhibit prolonged residence with the polymer substrate due to attractive chemical interactions with certain polymer functional groups [55,56]. The cumulative duration of exposure and partial pressure of the precursor vapor as well as the following purging step govern the precursor diffusion into the organic substrate, and thus the extent of infiltration.

In contrast, the growth of TiO_2 and SiO_2 proceeds through surface active sites due to the lower aggressiveness of $TiCl_4$ and $SiCl_4$ than TMA. This was reflected in their respective film thicknesses, as average TiO_2 and SiO_2 thicknesses of 15 and 10 nm were found after 50 and 100 cycles, respectively (see Fig. 2), significantly lower than the Al_2O_3 thickness of 20 nm after only 10 cycles. Moreover, the thicknesses calculated from the TiO_2 and SiO_2 wt. %, measured by ICP-OES, match well with the thicknesses observed under TEM (see Figure S3), confirming that both TiO_2 and SiO_2 grow at the surface. Assuming a linear growth with the number of cycles, growths per cycle (GPCs) of ~ 0.3 and ~ 10 nm can be estimated for TiO_2 and SiO_2 ALD (see Fig. 2 and S2). The GPC of TiO_2 is slightly higher than that typically reported for $TiCl_4/H_2O$ ALD, i.e., ~0.1 nm [57], likely due to remaining CVD components arising from the reaction of $TiCl_4$ with residual unpurged H_2O at nearly ambient conditions (see Figure S4a-b). Instead, the GPC of SiO_2 is in agreement with the 0.09–0.11 nm GPC reported for $SiCl_4/H_2O$ ALD [58,59], thereby suggesting the fully self-limiting behaviour of SiO_2 ALD even at nearly ambient conditions (see Figure S4c-d).

Polyethylene terephthalate (PET) films were fabricated by MLD using terephthaloyl chloride (TC) and ethylene glycol (EG). The average PET thickness was 1.5 nm after 50 cycles (see Fig. 2), which translates into a GPC of ~0.03 nm. Low GPCs of ~0.05–0.07 nm for PET MLD have already been reported [48,49,60], and are attributed to the tilted orientation of the polymer chains and double reaction terminations due to the bifunctional organic precursors, namely TC and EG [60,61]. The lower GPC value on budesonide than on OH–terminated substrates, such as TiO_2 nanoparticles and SiO_2 wafers, can be explained both by the lower number of surface OH groups on budesonide and by its hydrophobic nature as we will show later. Due to the fully organic composition of both the budesonide core and the PET film, elemental analysis to quantify the amount of deposited material is hardly possible. Yet, an estimation can be obtained from the measured film thickness according to Equation (S2). A PET loading of 1.1 wt. %, corresponding to a budesonide loading of 98.9%, was calculated (see Table S6 and Equation (S1)).

By combining an ALD metal precursor with an MLD bifunctional organic co-reactant, e.g., diol or dicarboxylic acid, hybrid inorganic/organic films can be manufactured. This class of materials is referred to as metal alkoxides or metalcones. Here, titanicone films were synthesized by using the ALD Ti precursor, $TiCl_4$, and the MLD co-reactant, EG. The average titanicone thickness was ~4.5 nm after 10 cycles and ~23 nm after 50 cycles (see Fig. 2, S2), corresponding to a GPC of ~0.45 nm. This GPC is consistent with that reported on Si wafers in a vacuum viscous-flow, hot-wall type reactor [62]. It is worth noting that chlorine impurities, due to incomplete reactions between $TiCl_4$ and EG possibly resulting from the steric hindrance of EG, and double reaction terminations due to the bifunctional nature of EG are expected in the titanicone film [62]. The Ti loading in the titanicone-coated budesonide after 50 cycles is 7.7%, considerably lower than the 12.7% found in the TiO_2-coated budesonide (see Table S5), despite the higher average thickness of the titanicone film. Hybrid films, in fact, contain

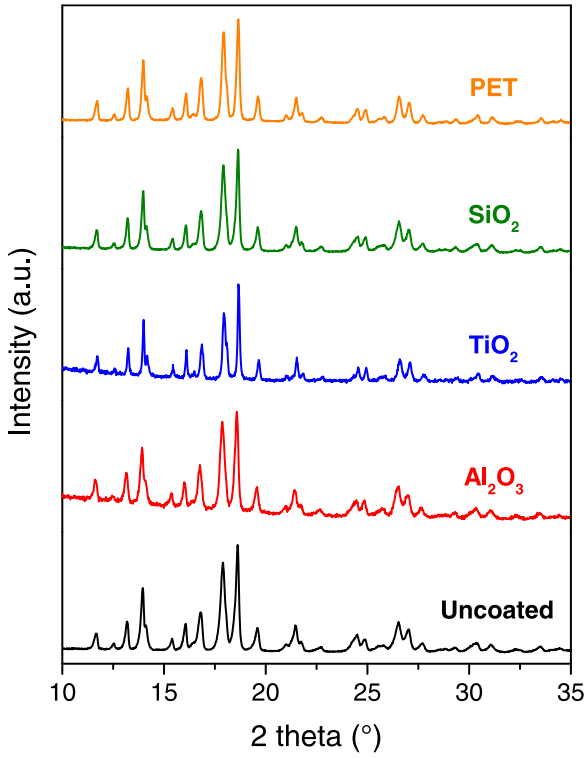

Fig. 3. XRPD diffractograms of uncoated, ALD-coated and MLD-coated budesonide particles.

a lower amount of metal than ALD films for the same thickness thanks to the lower film density arising from the presence of the organic component. In particular, the density of titanicone is found to be 1.8 g/cm^3 [62], whereas the lowest value reported for TiO_2 is 3.3 g/cm^3 [63]. This can be beneficial for pharmaceuticals where the inorganic content needs to be minimized.

3.2. Solid-state stability and cytocompatibility after ALD and MLD

To verify whether the chemical structure of the budesonide particles was stable upon the ALD and MLD processes, XRPD analysis was carried out (see Fig. 3). No difference is found in the diffractograms of uncoated, ALD-coated and MLD-coated budesonide, indicating the amorphous nature of the deposited films and more importantly the absence of noticeable variations in the solid-state structure of budesonide after the ALD and MLD processes, despite the use of highly reactive precursors. This is in agreement with our recent findings for Al_2O_3-coated lactose, where ultra-performance liquid chromatography (UPLC), XRPD and solid-state nuclear magnetic resonance (ssNMR) analyses demonstrated the chemical and structural integrity of the Al_2O_3-coated lactose particles [41]. In particular, no additional peak is found in the UPLC chromatogram of Al_2O_3-coated lactose compared to bare lactose, thus confirming that the Al_2O_3 ALD process does not induce decomposition of lactose. The lack of degradation upon the ALD process has also been shown in other ALD-coated pharmaceutical materials, such as acetaminophen, which maintained its stable polymorphic structure after Al_2O_3, TiO_2 and ZnO ALD [64], and indomethacin, which conserved its gamma (γ) polymorphic form after Al_2O_3 ALD [65]. Despite the limitation of XRPD in identifying only the crystalline phase of compounds, if above 1–2% by volume, the absence of changes in the diffractograms of uncoated and coated budesonide coupled with prior evidence from literature with various pharmaceuticals suggests the retention of the structural integrity of budesonide upon ALD and MLD.

The biocompatibility of inorganic and organic coatings has been investigated due to their use mainly in various biomedical implantable devices, such as cardiac pacemakers, cochlear implants, deep brain stimulations, neural prostheses and several physiological sensors, with the aim to protect against the fluidic environment and minimize the impact on the biological processes [66]. Moreover, the cytocompatibility of ALD coatings, including Al_2O_3 and TiO_2, onto pharmaceutical powders for oral administration and injection has been studied [64,65]. In particular, Al_2O_3 ALD films with a thickness of 30–35 nm and a loading of 17% did not result in any negative symptoms and inflammatory response in rats, demonstrating that Al_2O_3-coated indomethacin was safe and well tolerated for doses up to 100 mg/kg [65]. Analogously, Al_2O_3 ALD films up to 60 nm thick did not alter the proliferation of human coronary artery smooth muscle cells, suggesting good biocompatibility over a period of 7 days in-vitro [67]. In addition, Al_2O_3 ALD films onto glass slides and SiO_2 nanoparticles did not negatively interfere with the cellular viability of human dermal fibroblasts and human osteoblasts as well as did not activate the release of reactive oxygen species by macrophages [68]. Similarly, porous silicon microparticles coated by TiO_2 ALD were well tolerated by human dendritic cells, which play an essential role in the regulation of inflammatory and immune responses [69]. Furthermore, the incubation of human intestinal Caco-2 cells for 24 h with TiO_2-ALD-coated acetaminophen at concentrations up to 200 µg/mL did not induce any significant toxicity and reactive oxygen species [64]. Being generally non-toxic and biocompatible, SiO_2-based nanocapsules, such as mesoporous SiO_2 nanoparticles, have been fabricated to encapsulate bioactive molecules for bioimaging and controlled drug delivery [70,71]. Additionally, thermally grown SiO_2 films, for example by ALD, have been synthesized to create robust biofluid barriers for chronic electronic implants [72–74]. As also shown in the XRPD diffractograms in Fig. 3, ALD typically produces amorphous SiO_2, which is not considered harmful to people [75], as opposed to free crystalline silica, which is known to cause silicosis [76]. Animal inhalation studies with amorphous SiO_2 did not show any progressive fibrosis of the lungs nor any persistent silicotic nodules even in long-term experiments with high occupational exposures up to ~100 mg/m^3 [75]. Polymer-based matrices, such as polyether-ester copolymers partly consisting of PET, have been developed to encapsulate biologically active agents, e.g., proteins, peptides and small drug molecules, with the purpose of providing protection from degradation or denaturation and controlling release [77–79]. In-vitro and in-vivo studies in rabbits showed the biocompatibility of poly(ethylene glycol) terephthalate and poly(butylene terephthalate) (PEGT/PBT) copolymers [77]. Such copolymers have been also explored for tissue engineering applications, due to the possibility of manipulating the wettability, which is crucial in cell adhesion and growth, by tuning the PET content [80].

Most ALD oxide ceramics and MLD polymers are not expected to dissolve when in contact with body fluids, as they are not soluble in aqueous solutions at pH of interest. Still, insoluble material can be degraded and removed from the body through several clearance mechanisms. With respect to pulmonary delivery, insoluble inhaled material can be cleared in the alveolar region of the lung by phagocytosis via alveolar macrophages, which uptake and transport it towards the mucociliary escalator in the conducting airways, where the coordinated beating patterns of ciliated epithelial cells transport the mucus lining up the airway tree. Although oxide ceramics are widely used for several biomedical and drug delivery applications, as discussed above, their biocompatibility in formulations for inhaled delivery is not known yet. Cell viability tests using human epithelial alveolar A549 cells were thus performed with the budesonide powders coated by ALD oxide ceramic films. After incubation for 24 h of the A549 cells to concentrations

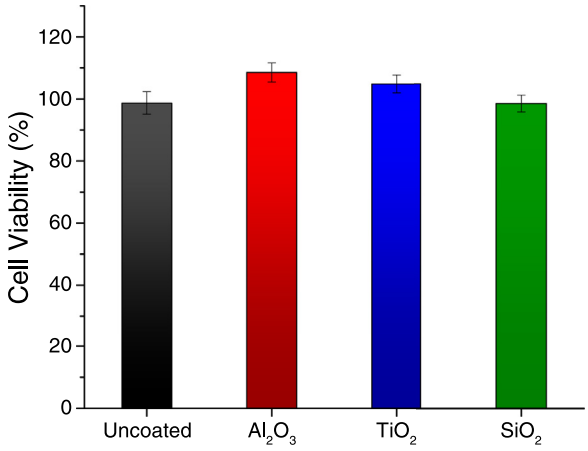

Fig. 4. Cell viability after treatment with a concentration of uncoated and ALD-coated budesonide of 100 µM for 24 h on human epithelial alveolar A549 cells. The values, expressed in %, are normalized with respect to the viability of untreated cells. The error bars indicate standard errors (n=15).

of uncoated and ALD-coated budesonide up to 100 µM, no toxicity is detected, and cell viability remains essentially constant at around 100% (see Fig. 4). Therefore, each ALD-coated budesonide formulation appears to be tolerated by human alveolar cells.

3.3. Effect of inorganic nanoscale films on budesonide wetting

The wettability of the uncoated and ALD-coated budesonide powders was first quantified by measuring the water contact angle (WCA). The WCA represents the angle formed at the three-phase boundary by a water droplet when placed and spread over the powder film. By following the evolution of WCA in the course of wetting, time effects such as evaporation are minimized, and local inhomogeneities in the powder film are averaged out. The powder can be classified as hydrophilic when WCA< 90°, hydrophobic when 90°<WCA< 145°, and superhydrophobic when WCA≥ 145° [81].

Fig. 5a and Figure S5 display the effect of the ALD ceramic films, Al_2O_3, TiO_2 and SiO_2, on the wetting of the budesonide powder. Uncoated budesonide shows strong hydrophobicity with a WCA of ~ 130°, which remains constant for the whole duration of the measurement, i.e., 5 min. Instead, a rapid, full transition to high hydrophilicity is observed for each ceramic material with a final contact angle close to 0°. The water droplet, in fact, soaks into the ALD-coated powder films within a few seconds, as shown in the pictures in Fig. 5a. No significant difference was found in the drop penetration time for Al_2O_3, TiO_2 and SiO_2, indicating a comparable hydrophilic behaviour. The consequence of the penetration of the water droplet into the powder film is the formation of a wet powder granule (see Figure S6). The morphology and size of the resulting granules give also insights into the wetting properties. In particular, the higher the hydrophilicity, the more the water droplet penetrates, and therefore the higher the granule size. In agreement with the contact angle, no noteworthy variation in the granule size of the ceramic-coated powders was found (see also Table S7). In addition, the granules appear to exhibit similar hardness when excavated from the powder film as well as comparable regular shapes. This is due to their strong structure which is not essentially susceptible to deformation upon external forces and due to the regular capillary path for liquid penetration in case of high hydrophilicity. Therefore, the morphology, size and hardness of the wet ALD-coated powder granules after the WCA measurements further suggest a similar hydrophilic character for Al_2O_3, TiO_2 and SiO_2.

We then investigated the dispersibility of the uncoated and ALD-coated budesonide powders in water. To avoid solubilization effects, saturated aqueous solutions of 1 mg/mL of budesonide powder were prepared. After mechanically mixing the powders in water for 1 min, it was observed that ALD-coated budesonide produced well-mixed dispersions as opposed to uncoated budesonide which did not properly disperse in water and mainly floated on the surface due to its hydrophobic nature (see Fig. 5b). To bet-

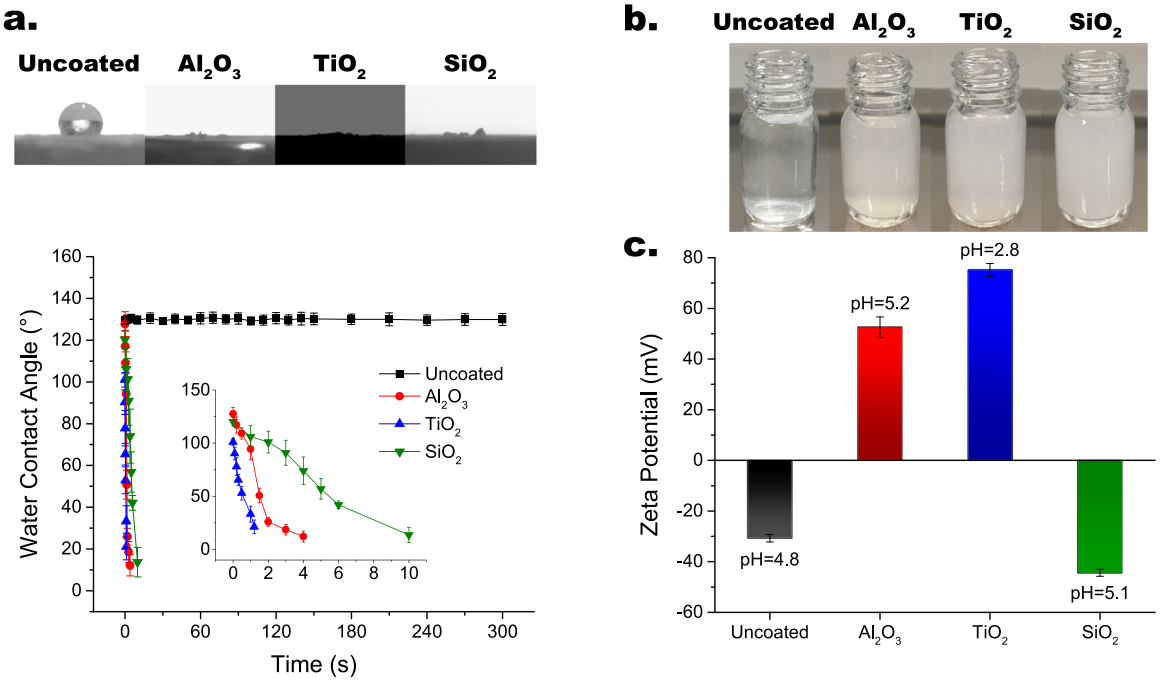

Fig. 5. Wetting of ALD-coated budesonide. (a) Water contact angle, (b) pictures after 1 min mixing in water and (c) zeta potential of uncoated and ALD-coated budesonide. The error bars indicate 95% confidence intervals.

ter quantify the dispersion stability, zeta potential measurements of the suspensions were conducted (see Fig. 5c). The zeta potential of the ALD-coated powder suspensions becomes either more negative, as in case of SiO_2-coated budesonide, or highly positive, as in case of Al_2O_3- and TiO_2- coated budesonide, compared to uncoated budesonide. No significant difference in pH was found in the Al_2O_3- and SiO_2- coated budesonide suspensions. Instead, the pH dropped from ~5 to ~3 for the TiO_2-coated budesonide suspension, likely due to the solubilization of chlorine-containing compounds arising from the $TiCl_4$ precursor. The lack of pH reduction in the SiO_2- coated budesonide suspension indicates the negligible amount of chlorine impurities in the SiO_2 film, despite the use of the $SiCl_4$ precursor at low temperature. In any case, the drastic change in zeta potential for each ALD-coated budesonide powder is a direct consequence of the ceramic films. In fact, Al_2O_3 at pH≃ 5 and TiO_2 at pH≃ 3 are positively charged, whereas SiO_2 is negatively charged at pH≃ 5 [82,83]. The zeta potential values of ALD-coated budesonide are therefore consistent with those reported in literature for Al_2O_3, TiO_2 and SiO_2 [82,83] as well as with the observed better dispersions.

Given the high wettability of ALD-coated budesonide, particle size distributions (PSDs) in water were measured to obtain a quantitative estimation of particle and agglomerate size, and their evolution with time. The PSD of uncoated budesonide shifts to higher sizes with increasing time, indicating its inherent hydrophobicity and tendency to agglomerate and float on the water surface (see Figure S7 and S11). In contrast, the PSDs of ALD-coated budesonide are nearly unaffected after 1 min, demonstrating the rapid and high degree of dispersion in water (see Figure S7). More precisely, we monitored the cumulative fraction of particles in two different size ranges, i.e., 0.1–10 μm and 10–1000 μm, over 5 min (see Fig. 6b,c). The higher the fraction of particles in the 0.1–10 μm range, which corresponds to the primary particle size range of budesonide, the better the dispersibility. Vice versa, the higher the fraction of agglomerates in the 10–1000 μm range, the poorer the dispersibility. After 2 min in water, the particle size ranges for each sample remain essentially constant, indicating that the suspensions are at steady state. The cumulative fraction of the ALD-coated particles in the 0.1–10 μm range rapidly increases from the onset of mixing and becomes nearly twice as high as that of uncoated budesonide (see Fig. 6b). Accordingly, the cumulative fraction of agglomerates in the 10–1000 μm range for ALD-coated budesonide significantly and quickly decreases over time, while it stays almost identical for uncoated budesonide (see Fig. 6c). Moreover, suspensions of ALD-coated budesonide after 1 h in water indicate their long-term stability (see Figure S8). The degree of dispersion from 1 min to 1 h remains essentially unaltered, without any powder sedimentation or agglomeration, thus suggesting no significant change in the PSD of ALD-coated budesonide suspensions in the long term. In summary, each ceramic ALD film modifies the surface characteristics of budesonide from hydrophobic to highly hydrophilic.

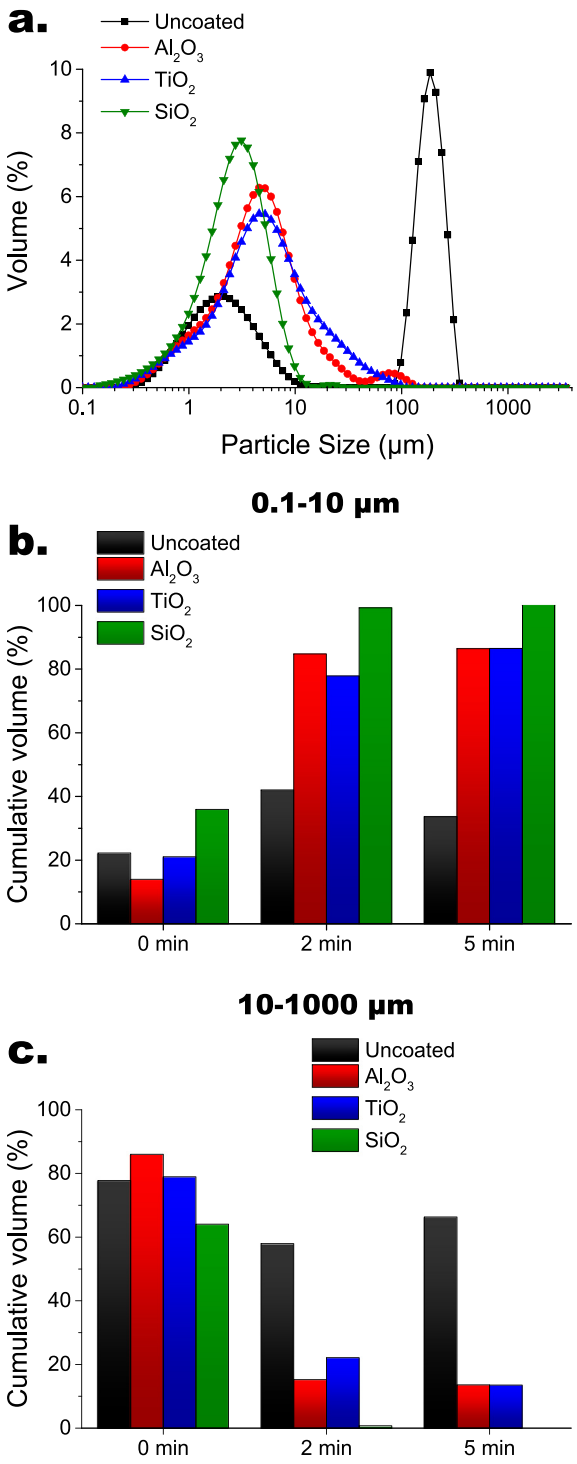

Fig. 6. Particle size distribution (PSD) of uncoated and ALD-coated budesonide particles in water. (a) Volume-based PSD after 2 min dispersing in water. (b) Cumulative volume fraction of particles in the 0.1–10 μm range at 0, 2 and 5 min dispersing in water. (c) Cumulative volume fraction of agglomerates in the 10–1000 μm range at 0, 2 and 5 min dispersing in water.

3.4. Effect of organic nanoscale films on budesonide wetting

Similarly, we examined the effect of organic components in purely organic MLD films, i.e., PET, and hybrid inorganic/organic ALD/MLD films, i.e., titanicone, on budesonide wettability. To that end, the WCA of PET-coated and titanicone-coated budesonide was measured (see Fig. 7a and Figure S9). PET-coated budesonide displays even higher hydrophobicity than uncoated budesonide with a WCA of ~145–150° making the powder superhydrophobic. The water droplet, in fact, stays intact over the measurement period of 5 min. Oh et al. showed that superhydrophobic PET fabrics can be obtained by adding a thermal ageing step at ≥130 °C to alkaline hydrolysis [84]. In particular, the surface of alkaline hydrolyzed PET fabric, which possesses many polar groups, naturally tends to minimize the surface energy, and above the glass transition temperature promotes the reorientation of polymer chains through migration of the polar groups into the PET bulk. Analogously, the PET films grown at 150 °C might spontaneously decrease the free energy of the interface by diffusing the polar groups into the film, thus resulting in surface superhydrophobicity. However, due to in-

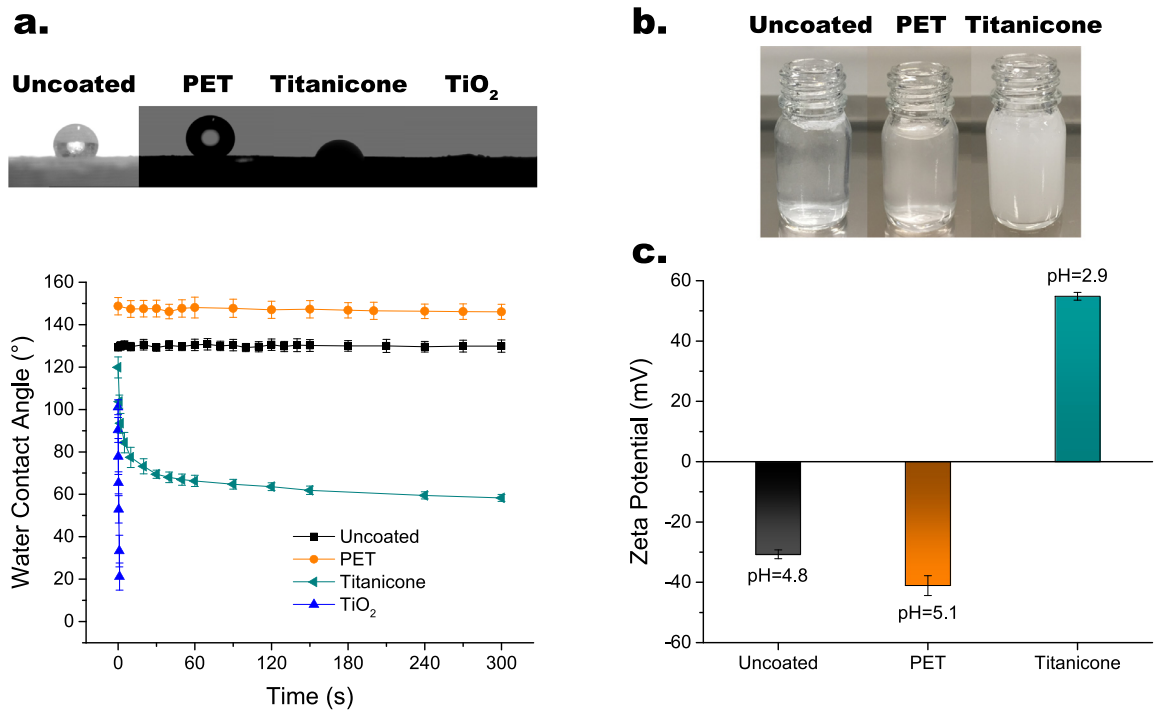

Fig. 7. Wetting of MLD and hybrid ALD-MLD coated budesonide. (a) Water contact angle, (b) pictures after 1 min mixing in water and (c) zeta potential of uncoated, and MLD and hybrid ALD-MLD coated budesonide. The error bars indicate 95% confidence intervals.

herent imperfections of ultrathin polymer films such as in the case of ~1.5 nm PET, sub-nanoscale surface roughness effects might also play a role.

On the other hand, the titanicone-coated budesonide exhibits a more hydrophilic character than uncoated budesonide, with a stable WCA after 5 min of ~ 80° and ~ 60° for the 10 and 50 cycles samples, respectively (see Figure S10). Hence, no high hydrophilicity was observed, as the water droplet was not able to fully spread into the powder film. This is attributed to the competition between the inorganic and organic structures. It is worth noting that the WCA mainly varies in the first minute, and then is effectively stable. This WCA profile could be explained by the instability of metalcones in water [85–88]. Upon soaking titanicone-coated particles in water, Patel et al. reported the formation of micropores with a diameter of ~0.6 nm and mesopores of ~1.1 nm in the film, leading to the removal of the organic components, i.e., EG chains, as evidenced by the substantial increase in surface area, and to the loss of film conformality [87].

Furthermore, they tested the stability of the titanicone-coated particles to water vapor. FTIR spectra revealed the disappearance of the peaks related to $-CH_3$, $-CH_2$ and alkene groups after 24 h exposure, indicating the decomposition of the organic components in the titanicone films, which were essentially converted into titania [87]. Therefore, the water droplet during the WCA measurements may cause modifications in the chemical structure of titanicone through decomposition of the organic fraction, leading to a slight shrinkage in the film thickness and, more importantly, to a porous structure that includes both the hydrophobic contribution from budesonide and the hydrophilic contribution from TiO_x species. Such effects result, in fact, in a WCA in between that of uncoated and MLD-coated budesonide, and that of ALD-coated budesonide, which tends to decrease with increasing TiO_x fractions.

When dispersing the PET-coated budesonide in water, it created more stable suspensions than uncoated budesonide, despite the higher hydrophobicity (see Fig. 7b). This behavior was already observed in aqueous supensions with PET-coated TiO_2 nanoparticles, which could remain dispersed for several hours compared to uncoated TiO_2 that sedimented within 3 hours [48]. The PET films, in fact, stabilize the few particles in suspension by electrostatic repulsion, thus reducing the extent of aggregation and delaying their sedimentation. However, the majority of powder in the PET-coated budesonide suspension still floats on the water surface after 1 min mixing, as in the case of uncoated budesonide (see Figure S11). Instead, titanicone-coated budesonide delivered stable suspensions (see Fig. 7b), in agreement with the WCA measurements. It is worth noting that even the titanicone-coated budesonide suspension still exhibits a tiny fraction of powder floating on the water surface after 1 min mixing (see Figure S11), likely due to its mild hydrophilicity. Zeta potential measurements are in line with the direct observations of the suspensions. In particular, the zeta potential of PET-coated budesonide drops to -41.1 mV, whereas that of titanicone-coated budesonide increases to 54.9 mV (see Fig. 7c). Both the decrease in zeta potential and the absence of meaningful variation in pH for the PET-coated powder suspension are consistent with our previous study on PET-coated TiO_2 nanoparticles [48]. At pH≃ 5, in fact, PET is highly negatively charged [89,90], thus causing the zeta potential to drop. Instead, the increase in zeta potential and the decrease in pH for the titanicone-coated budesonide suspension follow the trend for TiO_2-coated budesonide. This may also suggest the conversion of titanicone into TiO_2, driven by the decomposition of the organic components, when soaked in water [87]. Contrary to titanicone and generally to hybrid ALD/MLD films, the MLD-grown PET films are stable in water [48], thanks to their good chemical resistance.

It is well known that the wetting properties of surfaces strongly depend on both their chemical composition and physical structure. The synthesis of smooth nanoscale films by ALD, MLD and hybrid ALD/MLD minimizes any physical effect on the substrate surface, and therefore differences are primarily attributed to the surface chemical composition, which is tuned at the atomic or molecular level. ALD, which typically manufactures ceramics such as Al_2O_3, TiO_2 and SiO_2 that are generally highly hydrophilic due to the

presence of metal cations, oxygen anions, and hydroxyl groups on the surface, can transform hydrophobic materials to completely hydrophilic. On the other hand, MLD, which fabricates organic polymers that are typically hydrophobic, can be used to obtain superhydrophobic materials due to the reorientation of the polymer chains when operating at reaction temperatures above their glass transition temperature or due to sub-nanoscale surface roughness. The combination of ALD and MLD in hybrid ALD/MLD can instead deliver mildly hydrophilic properties thanks to the hydrophobicity of the organic components and the hydrophilicity of ceramic species. The instability of hybrid films made of short aliphatic organic chains, e.g., EG, upon exposure to water can be beneficial for controlled wettability applications, as it brings about the formation of porous structures with properties both of the converted inorganic fraction in the porous film and of the substrate. Furthermore, the wide spectrum of organic precursors available from organic chemistry can be harnessed to obtain a large variety of film properties. For instance, aromatic organic precursors such as 4-aminophenol and 4,4'-oxydianiline can result in hybrid films with good stability to both atmospheric air and water [91,92], in case porous films are not desirable. In addition, by combining hybrid ALD/MLD with ALD, the inorganic and organic fractions in hybrid films can be adjusted, and finer tuning of the wettability can be achieved. In the context of pharmaceutical applications, it is important to stress that nanoscale films only lead to the addition of minute amounts of guest material even on drug particles with a moderate surface area such as micronized budesonide. For instance, in this study, we obtained highly hydrophilic powders with drug loadings up to ~95% (see Tables S2 to S4) as well as superhydrophobic powders with an estimated drug loading of ~99% (see Table S6). This makes ALD, MLD and hybrid ALD/MLD highly attractive for altering the wetting properties of pharmaceutical powders. Moreover, our approach using fluidized bed reactors is very efficient with respect to precursor utilization [93] as well as easily scalable [94], especially in the pharmaceutical industry where they are well-established technologies.

4. Conclusion

In summary, we have fine-tuned the wettability of drug powders with inorganic, organic and inorganic/organic nanoscale films deposited by ALD, MLD and hybrid ALD/MLD, respectively. TEM shows the deposition of uniform Al_2O_3, TiO_2, SiO_2, PET and titanicone films on each individual budesonide particle. While Al_2O_3 infiltrates into the budesonide structure forming an Al_2O_3-budesonide shell, the growth of TiO_2, SiO_2, PET and titanicone proceeds through surface active sites with GPCs of ~0.3, ~0.1, ~0.03 and ~0.45 nm, respectively. Importantly, the budesonide particles retain their solid-state structure and cytocompatibility after the deposition processes. The uncoated budesonide powder is hydrophobic with an average WCA of 130°. The ceramic ALD films, i.e., Al_2O_3, TiO_2 and SiO_2, are able to deliver highly hydrophilic budesonide powders with WCAs close to 0° within a few seconds. Instead, organic components in the MLD and hybrid ALD/MLD films alter the wetting properties from superhydrophobic (WCA= 145–150°) for purely organic films, i.e., PET, to mildly hydrophilic (WCA= 60–80°) for inorganic-organic films, i.e., titanicone. In the case of ALD, such effects are attributed to the drastic change in the surface chemical composition rather than in the surface physical structure, which remains essentially unaffacted after the deposition processes. On the other hand, in the case of hybrid ALD/MLD with short aliphatic organic co-reactants unstable in water, e.g., EG, the formation of porous inorganic-organic structures upon contact with water may be behind the mild hydrophilicity. In the case of PET MLD, diffusion of the polar groups into the film by reorientation of the polymer chains or sub-nanoscale surface roughness can explain the surface superhydrophobicity. The ability of ALD, MLD and hybrid ALD/MLD to provide the whole spectrum of wettability control for drug powders from high hydrophilicity to superhydrophobicity is relevant for improving bioavailability for example in pulmonary delivery, enhancing the dispersion of liquid-based medical products or preventing moisture ingress in solid sensitive pharmaceuticals. Hybrid films can be preferable over their ceramic counterparts for pharmaceutical formulations where initially mild hydrophilicity is sufficient but lower metal content is required. Finally, tailoring the wetting properties at the nanoscale can be of interest to several applications such as food, paints and cosmetics.

5. Supplementary material

Experimental conditions; WCA setup; Al, Ti, Si and budesonide loadings in ALD-coated and hybrid-coated budesonide; estimated PET loading in MLD-coated budesonide; TEM images of budesonide after 10 cycles of Al_2O_3, TiO_2 and titanicone; estimated film thickness from Al_2O_3, TiO_2 and SiO_2 wt. %; saturation behaviour of TiO_2 and SiO_2 ALD; WCA of budesonide after 10 cycles of Al_2O_3 and TiO_2; wet granules of ALD-coated budesonide; PSDs of ALD-coated budesonide in water at different time points; ALD-coated budesonide suspensions after 1 h; water droplet evolution during WCA of MLD-coated and hybrid-coated budesonide; WCA of budesonide after 10 cycles of titanicone; top view of uncoated, MLD-coated and hybrid-coated budesonide suspensions in water.

Supplementary material associated with this article can be found, in the online version, at doi:10.1016/j.apmt.2021.100945.

6. Data availability

The raw/processed data required to reproduce these findings cannot be shared at this time as the data also forms part of an ongoing study.

Declaration of Competing Interest

J.R. van Ommen has a financial interest in Delft IMP.

CRediT authorship contribution statement

Damiano La Zara: Conceptualization, Methodology, Formal analysis, Validation, Investigation, Data curation, Writing - original draft, Writing - review & editing, Visualization. **Fuweng Zhang:** Conceptualization, Methodology, Formal analysis, Validation, Investigation, Writing - original draft, Writing - review & editing. **Feilong Sun:** Validation, Investigation, Writing - review & editing. **Maximilian R. Bailey:** Investigation, Writing - review & editing. **Michael J. Quayle:** Conceptualization, Resources, Supervision, Project administration, Funding acquisition. **Gunilla Petersson:** Conceptualization, Resources, Writing - review & editing, Supervision, Project administration, Funding acquisition. **Staffan Folestad:** Conceptualization, Resources, Supervision, Project administration, Funding acquisition. **J. Ruud van Ommen:** Conceptualization, Resources, Writing - review & editing, Supervision, Project administration, Funding acquisition.

Acknowledgements

The authors thank Vera Wissel for part of the ALD experiments, DelftIMP for the hybrid ALD/MLD experiments, Delft Solids Solutions for the particle size distributions and Robin Ras for insightful comments. Furthermore, the authors acknowledge the financial support from AstraZeneca and Health~Holland, Top Sector Life Sciences & Health, to stimulate public-private partnerships.

References

[1] B.C. Lippold, A. Ohm, Correlation between wettability and dissolution rate of pharmaceutical powders, Int. J. Pharm. 28 (1) (1986) 67–74, doi:10.1016/0378-5173(86)90148-1.

[2] P. Buch, C. Meyer, P. Langguth, Improvement of the wettability and dissolution of fenofibrate compacts by plasma treatment, Int. J. Pharm. 416 (1) (2011) 49–54, doi:10.1016/j.ijpharm.2011.05.074.

[3] Y. Lu, N. Tang, R. Lian, J. Qi, W. Wu, Understanding the relationship between wettability and dissolution of solid dispersion, Int. J. Pharm. 465 (1–2) (2014) 25–31, doi:10.1016/j.ijpharm.2014.02.004.

[4] H. Takasaki, E. Yonemochi, R. Messerschmid, M. Ito, K. Wada, K. Terada, Importance of excipient wettability on tablet characteristics prepared by moisture activated dry granulation (MADG), Int. J. Pharm. 456 (1) (2013) 58–64, doi:10.1016/j.ijpharm.2013.08.027.

[5] B. Yang, L. Xu, Q. Wang, S. Li, Modulation of the wettability of excipients by surfactant and its impacts on the disintegration and release of tablets, Drug Dev. Ind. Pharm. 42 (12) (2016) 1945–1955, doi:10.1080/03639045.2016.1185436.

[6] B. Yang, C. Wei, Y. Yang, Q. Wang, S. Li, Evaluation about wettability, water absorption or swelling of excipients through various methods and the correlation between these parameters and tablet disintegration, Drug Dev. Ind. Pharm. 44 (9) (2018) 1417–1425, doi:10.1080/03639045.2018.1453519.

[7] C.L.-N. Vo, C. Park, B.-J. Lee, Current trends and future perspectives of solid dispersions containing poorly water-soluble drugs, Eur. J. Pharm. Biopharm. 85 (3) (2013) 799–813, doi:10.1016/j.ejpb.2013.09.007.

[8] D. Zhang, J. Flory, S. Panmai, U. Batra, M. Kaufman, Wettability of pharmaceutical solids: its measurement and influence on wet granulation, Colloids Surf., A 206 (1–3) (2002) 547–554, doi:10.1016/s0927-7757(02)00091-2.

[9] E. Pallagi, K. Karimi, R. Ambrus, P. Szabó-Révész, I. Csóka, New aspects of developing a dry powder inhalation formulation applying the quality-by-design approach, Int. J. Pharm. 511 (1) (2016) 151–160, doi:10.1016/j.ijpharm.2016.07.003.

[10] L. Lin, G. Quan, T. Peng, Z. Huang, V. Singh, M. Lu, C. Wu, Development of fine solid-crystal suspension with enhanced solubility, stability, and aerosolization performance for dry powder inhalation, Int. J. Pharm. 533 (1) (2017) 84–92, doi:10.1016/j.ijpharm.2017.09.024.

[11] G. Buckton, The influence of additives on the recrystallisation of amorphous spray dried lactose, Int. J. Pharm. 121 (1) (1995) 81–87, doi:10.1016/0378-5173(95)00009-8.

[12] H.-K. Chain, I. Gonda, Solid state characterization of spray-dried powders of recombinant human deoxyribonuclease (rhdnase)†, J. Pharm. Sci. 87 (5) (1998) 647–654, doi:10.1021/js9504292.

[13] K. Stank, H. Steckel, Physico-chemical characterisation of surface modified particles for inhalation, Int. J. Pharm. 448 (1) (2013) 9–18, doi:10.1016/j.ijpharm.2013.03.009.

[14] P.B. Myrdal, P. Sheth, S.W. Stein, Advances in metered dose inhaler technology: formulation development, AAPS PharmSciTech 15 (2) (2014) 434–455, doi:10.1208/s12249-013-0063-x.

[15] L. Chen, T. Okuda, X.-Y. Lu, H.-K. Chan, Amorphous powders for inhalation drug delivery, Adv. Drug Deliv. Rev. 100 (2016) 102–115, doi:10.1016/j.addr.2016.01.002.

[16] M.J. Telko, A.J. Hickey, Dry powder inhaler formulation, Respir. Care 50 (9) (2005) 1209–1227.

[17] R. Pfeffer, R.N. Dave, D. Wei, M. Ramlakhan, Synthesis of engineered particulates with tailored properties using dry particle coating, Powder Technol. 117 (1–2) (2001) 40–67, doi:10.1016/s0032-5910(01)00314-x.

[18] V. Karde, C. Ghoroi, Influence of surface modification on wettability and surface energy characteristics of pharmaceutical excipient powders, Int. J. Pharm. 475 (1–2) (2014) 351–363, doi:10.1016/j.ijpharm.2014.09.002.

[19] V. Karde, S. Panda, C. Ghoroi, Surface modification to improve powder bulk behavior under humid conditions, Powder Technol. 278 (2015) 181–188, doi:10.1016/j.powtec.2015.03.025.

[20] E.Z. Dahmash, A.R. Mohammed, Functionalised particles using dry powder coating in pharmaceutical drug delivery: promises and challenges, Expert Opin. Drug Deliv. 12 (12) (2015) 1867–1879, doi:10.1517/17425247.2015.1071351.

[21] S. Varghese, C. Ghoroi, Improving the wetting and dissolution of ibuprofen using solventless co-milling, Int. J. Pharm. 533 (1) (2017) 145–155, doi:10.1016/j.ijpharm.2017.09.062.

[22] D. Dixit, S. Bunk, R. Rane, C. Ghoroi, Influence of ar plasma treatment on the wetting behavior of pharmaceutical powders, Adv. Powder Technol. 29 (12) (2018) 2928–2940, doi:10.1016/j.apt.2018.09.015.

[23] S. Watano, H. Nakamura, K. Hamada, Y. Wakamatsu, Y. Tanabe, R.N. Dave, R. Pfeffer, Fine particle coating by a novel rotating fluidized bed coater, Powder Technol. 141 (3) (2004) 172–176, doi:10.1016/j.powtec.2003.03.001.

[24] S. Bose, R.H. Bogner, Solventless pharmaceutical coating processes: a review, Pharm. Dev. Technol. 12 (2) (2007) 115–131, doi:10.1080/10837450701212479.

[25] C.-Y. Leung, A.N. Trementozzi, Y. Lin, J. Xu, E. Irdam, J.M. MacPhee, M. He, S.B. Karki, P. Boulas, P.N. Zawaneh, Enteric coating of micron-size drug particles through a würster fluid-bed process, Powder Technol. 317 (2017) 247–252, doi:10.1016/j.powtec.2017.04.046.

[26] N. Pearnchob, R. Bodmeier, Dry polymer powder coating and comparison with conventional liquid-based coatings for eudragit® RS, ethylcellulose and shellac, Eur. J. Pharm. Biopharm. 56 (3) (2003) 363–369, doi:10.1016/s0939-6411(03)00121-8.

[27] J. Raula, J. Seppälä, J. Malm, M. Karppinen, E.I. Kauppinen, Structure and dissolution of l-leucine-coated salbutamol sulphate aerosol particles, AAPS PharmSciTech 13 (2) (2012) 707–712, doi:10.1208/s12249-012-9789-0.

[28] A. Perrotta, O. Werzer, A.M. Coclite, Strategies for drug encapsulation and controlled delivery based on vapor-phase deposited thin films, Adv. Eng. Mater. 20 (3) (2017) 1700639, doi:10.1002/adem.201700639.

[29] J. Raula, A. Lähde, E.I. Kauppinen, A novel gas phase method for the combined synthesis and coating of pharmaceutical particles, Pharm. Res. 25 (1) (2007) 242–245, doi:10.1007/s11095-007-9464-4.

[30] K.K. Lau, K.K. Gleason, Particle functionalization and encapsulation by initiated chemical vapor deposition (icvd), Surf. Coat. Technol. 201 (22–23) (2007) 9189–9194, doi:10.1016/j.surfcoat.2007.04.045.

[31] H.V. Bui, F. Grillo, J.R. van Ommen, Atomic and molecular layer deposition: off the beaten track, Chem. Commun. 53 (1) (2017) 45–71, doi:10.1039/c6cc05568k.

[32] X. Meng, An overview of molecular layer deposition for organic and organic–inorganic hybrid materials: mechanisms, growth characteristics, and promising applications, J. Mater. Chem. A 5 (35) (2017) 18326–18378, doi:10.1039/c7ta04449f.

[33] M. Kemell, E. Färm, M. Ritala, M. Leskelä, Surface modification of thermoplastics by atomic layer deposition of Al_2O_3 and TiO_2 thin films, Eur. Polym. J. 44 (11) (2008) 3564–3570, doi:10.1016/j.eurpolymj.2008.09.005.

[34] G.K. Hyde, G. Scarel, J.C. Spagnola, Q. Peng, K. Lee, B. Gong, K.G. Roberts, K.M. Roth, C.A. Hanson, C.K. Devine, S.M. Stewart, D. Hojo, J.-S. Na, J.S. Jur, G.N. Parsons, Atomic layer deposition and abrupt wetting transitions on nonwoven polypropylene and woven cotton fabrics, Langmuir 26 (4) (2010) 2550–2558, doi:10.1021/la902830d.

[35] G.K. Hyde, S.M. Stewart, G. Scarel, G.N. Parsons, C.-C. Shih, C.-M. Shih, S.-J. Lin, Y.-Y. Su, N.A. Monteiro-Riviere, R.J. Narayan, Atomic layer deposition of titanium dioxide on cellulose acetate for enhanced hemostasis, Biotechnol. J. 6 (2) (2011) 213–223, doi:10.1002/biot.201000342.

[36] K. Lee, J.S. Jur, D.H. Kim, G.N. Parsons, Mechanisms for hydrophilic/hydrophobic wetting transitions on cellulose cotton fibers coated using Al_2O_3 atomic layer deposition, J. Vacuum Sci. Technol. A: Vacuum, Surf. Films 30 (1) (2012) 01A163, doi:10.1116/1.3671942.

[37] M. Shimel, I. Gouzman, E. Grossman, Z. Barkay, S. Katz, A. Bolker, N. Eliaz, R. Verker, Enhancement of wetting and mechanical properties of UHMWPE-based composites through alumina atomic layer deposition, Adv. Mater. Interfaces 5 (14) (2018) 1800295, doi:10.1002/admi.201800295.

[38] Y. Ding, S. Xu, Y. Zhang, A.C. Wang, M.H. Wang, Y. Xiu, C.P. Wong, Z.L. Wang, Modifying the anti-wetting property of butterfly wings and water strider legs by atomic layer deposition coating: surface materials versus geometry, Nanotechnology 19 (35) (2008) 355708, doi:10.1088/0957-4484/19/35/355708.

[39] A.I. Abdulagatov, F.F. Orudzhev, M.K. Rabadanov, I.M. Abdulagatov, Copper nanowire arrays surface wettability control using atomic layer deposition of TiO_2, Russ. J. Appl. Chem. 89 (8) (2016) 1265–1273, doi:10.1134/s1070427216080085.

[40] D. Zhang, M.J. Quayle, G. Petersson, J.R. van Ommen, S. Folestad, Atomic scale surface engineering of micro- to nano-sized pharmaceutical particles for drug delivery applications, Nanoscale 9 (32) (2017) 11410–11417, doi:10.1039/c7nr03261g.

[41] D. Zhang, D. La Zara, M.J. Quayle, G. Petersson, J.R. van Ommen, S. Folestad, Nanoengineering of crystal and amorphous surfaces of pharmaceutical particles for biomedical applications, ACS Appl. Bio Mater. 2 (4) (2019) 1518–1530, doi:10.1021/acsabm.8b00805.

[42] A.E. Short, S.V. Pamidi, Z.E. Bloomberg, Y. Li, M.D. Losego, Atomic layer deposition (ALD) of subnanometer inorganic layers on natural cotton to enhance oil sorption performance in marine environments, J. Mater. Res. 34 (4) (2019) 563–570, doi:10.1557/jmr.2018.441.

[43] Y. Li, L. Chen, J.P. Wooding, F. Zhang, R.P. Lively, R. Ramprasad, M.D. Losego, Controlling wettability, wet strength, and fluid transport selectivity of nanopaper with atomic layer deposited (ALD) sub-nanometer metal oxide coatings, Nanoscale Adv. 2 (1) (2020) 356–367, doi:10.1039/c9na00417c.

[44] J. Malm, E. Sahramo, M. Karppinen, R.H.A. Ras, Photo-controlled wettability switching by conformal coating of nanoscale topographies with ultrathin oxide films, Chem. Mater. 22 (11) (2010) 3349–3352, doi:10.1021/cm903831c.

[45] Y. Huang, G. Pandraud, P.M. Sarro, Characterization of low temperature deposited atomic layer deposition TiO_2 for MEMS applications, J. Vacuum Sci. Technol. A: Vacuum, Surf. Films 31 (1) (2013) 01A148, doi:10.1116/1.4772664.

[46] S. Hoshian, V. Jokinen, K. Hjort, R.H.A. Ras, S. Franssila, Amplified and localized photoswitching ofTiO_2 by micro- and nanostructuring, ACS Appl. Mater. Interfaces 7 (28) (2015) 15593–15599, doi:10.1021/acsami.5b04309.

[47] Y. Chen, B. Zhang, Z. Gao, C. Chen, S. Zhao, Y. Qin, Functionalization of multiwalled carbon nanotubes with uniform polyurea coatings by molecular layer deposition, Carbon N Y 82 (2015) 470–478, doi:10.1016/j.carbon.2014.10.090.

[48] D. La Zara, M.R. Bailey, P.-L. Hagedoorn, D. Benz, M.J. Quayle, S. Folestad, J.R. van Ommen, Sub-nanoscale surface engineering of TiO_2 nanoparticles by molecular layer deposition of poly(ethylene terephthalate) for suppressing photoactivity and enhancing dispersibility, ACS Appl. Nano Mater. 3 (7) (2020) 6737–6748, doi:10.1021/acsanm.0c01158.

[49] J. Gil-Font, M.-A. Hatte, M.R. Bailey, N. Navarrete, J. Ventura-Espinosa, A. Goulas, D. La Zara, J.R. van Ommen, R. Mondragón, L. Hernández, Improving heat transfer of stabilised thermal oil-based tin nanofluids using biosurfactant and molecular layer deposition, Appl. Therm. Eng. 178 (2020) 115559, doi:10.1016/j.applthermaleng.2020.115559.

[50] C. Albert, M. Beladjine, N. Tsapis, E. Fattal, F. Agnely, N. Huang, Pickering emulsions: preparation processes, key parameters governing their properties and potential for pharmaceutical applications, J. Controlled Release 309 (2019) 302–332, doi:10.1016/j.jconrel.2019.07.003.

[51] W.L. Chiou, S. Riegelman, Pharmaceutical applications of solid dispersion systems, J. Pharm. Sci. 60 (9) (1971) 1281–1302, doi:10.1002/jps.2600600902.

[52] T. Nguyen, W. Shen, K. Hapgood, Drop penetration time in heterogeneous powder beds, Chem. Eng. Sci. 64 (24) (2009) 5210–5221, doi:10.1016/j.ces.2009.08.038.

[53] J. Ji, J. Fitzpatrick, K. Cronin, P. Maguire, H. Zhang, S. Miao, Rehydration behaviours of high protein dairy powders: the influence of agglomeration on wettability, dispersibility and solubility, Food Hydrocoll. 58 (2016) 194–203, doi:10.1016/j.foodhyd.2016.02.030.

[54] S. Wu, J. Fitzpatrick, K. Cronin, V. Maidannyk, S. Miao, Effects of spraying surfactants in a fluidised bed on the rehydration behaviour of milk protein isolate powder, J. Food Eng. 266 (2020) 109694, doi:10.1016/j.jfoodeng.2019.109694.

[55] S.-M. Lee, E. Pippel, U. Gosele, C. Dresbach, Y. Qin, C.V. Chandran, T. Brauniger, G. Hause, M. Knez, Greatly increased toughness of infiltrated spider silk, Science 324 (5926) (2009) 488–492, doi:10.1126/science.1168162.

[56] R.Z. Waldman, D.J. Mandia, A. Yanguas-Gil, A.B.F. Martinson, J.W. Elam, S.B. Darling, The chemical physics of sequential infiltration synthesis—a thermodynamic and kinetic perspective, J. Chem. Phys. 151 (19) (2019) 190901, doi:10.1063/1.5128108.

[57] J.-P. Niemelä, G. Marin, M. Karppinen, Titanium dioxide thin films by atomic layer deposition: a review, Semicond. Sci. Technol. 32 (9) (2017) 093005, doi:10.1088/1361-6641/aa78ce.

[58] J.D. Ferguson, A.W. Weimer, S.M. George, Atomic layer deposition of SiO_2 films on BN particles using sequential surface reactions, Chem. Mater. 12 (11) (2000) 3472–3480, doi:10.1021/cm000313t.

[59] O. Sneh, M. Wise, A. Ott, L. Okada, S. George, Atomic layer growth of SiO_2 on Si(100) using $SiCl_4$ and H_2O in a binary reaction sequence, Surf. Sci. 334 (1–3) (1995) 135–152, doi:10.1016/0039-6028(95)00471-8.

[60] T.V. Ivanova, P.S. Maydannik, D.C. Cameron, Molecular layer deposition of polyethylene terephthalate thin films, J. Vacuum Sci. Technol. A: Vacuum, Surf. Films 30 (1) (2012) 01A121, doi:10.1116/1.3662846.

[61] D.S. Bergsman, R.G. Closser, C.J. Tassone, B.M. Clemens, D. Nordlund, S.F. Bent, Effect of backbone chemistry on the structure of polyurea films deposited by molecular layer deposition, Chem. Mater. 29 (3) (2017) 1192–1203, doi:10.1021/acs.chemmater.6b04530.

[62] A.I. Abdulagatov, R.A. Hall, J.L. Sutherland, B.H. Lee, A.S. Cavanagh, S.M. George, Molecular layer deposition of titanicone films using $TiCl_4$ and ethylene glycol or glycerol: growth and properties, Chem. Mater. 24 (15) (2012) 2854–2863, doi:10.1021/cm300162v.

[63] B.D. Piercy, C.Z. Leng, M.D. Losego, Variation in the density, optical polarizabilities, and crystallinity of TiO_2 thin films deposited via atomic layer deposition from 38 to 150°C using the titanium tetrachloride-water reaction, J. Vacuum Sci. Technol. A: Vacuum, Surf. Films 35 (3) (2017) 03E107, doi:10.1116/1.4979047.

[64] T.O. Kääriäinen, M. Kemell, M. Vehkamäki, M.-L. Kääriäinen, A. Correia, H.A. Santos, L.M. Bimbo, J. Hirvonen, P. Hoppu, S.M. George, D.C. Cameron, M. Ritala, M. Leskelä, Surface modification of acetaminophen particles by atomic layer deposition, Int. J. Pharm. 525 (1) (2017) 160–174, doi:10.1016/j.ijpharm.2017.04.031.

[65] J. Hellrup, M. Rooth, E. Mårtensson, K. Sigfridsson, A. Johansson, Nanoshells prepared by atomic layer deposition – long acting depots of indomethacin, Eur. J. Pharm. Biopharm. 140 (2019) 60–66, doi:10.1016/j.ejpb.2019.04.019.

[66] S.-H. Ahn, J. Jeong, S.J. Kim, Emerging encapsulation technologies for long-term reliability of microfabricated implantable devices, Micromachines (Basel) 10 (8) (2019) 508, doi:10.3390/mi10080508.

[67] D.S. Finch, T. Oreskovic, K. Ramadurai, C.F. Herrmann, S.M. George, R.L. Mahajan, Biocompatibility of atomic layer-deposited alumina thin films, J. Biomed. Mater. Res. Part A 87A (1) (2008) 100–106, doi:10.1002/jbm.a.31732.

[68] G. Mestres, M. Espanol, W. Xia, M. Tenje, M. Ott, Evaluation of biocompatibility and release of reactive oxygen species of aluminum oxide-coated materials, ACS Omega 1 (4) (2016) 706–713, doi:10.1021/acsomega.6b00198.

[69] E. Chistè, A. Ghafarinazari, M. Donini, V. Cremers, J. Dendooven, C. Detavernier, D. Benati, M. Scarpa, S. Dusi, N. Daldosso, TiO_2-Coated luminescent porous silicon micro-particles as a promising system for nanomedicine, J. Mater. Chem. B 6 (12) (2018) 1815–1824, doi:10.1039/c7tb02614e.

[70] Y. Zhang, B.Y.W. Hsu, C. Ren, X. Li, J. Wang, Silica-based nanocapsules: synthesis, structure control and biomedical applications, Chem. Soc. Rev. 44 (1) (2015) 315–335, doi:10.1039/c4cs00199k.

[71] F. Tang, L. Li, D. Chen, Mesoporous silica nanoparticles: synthesis, biocompatibility and drug delivery, Adv. Mater. 24 (12) (2012) 1504–1534, doi:10.1002/adma.201104763.

[72] J. Jeong, F. Laiwalla, J. Lee, R. Ritasalo, M. Pudas, L. Larson, V. Leung, A. Nurmikko, Conformal hermetic sealing of wireless microelectronic implantable chiplets by multilayered atomic layer deposition (ALD), Adv. Funct. Mater. (2018) 1806440, doi:10.1002/adfm.201806440.

[73] H. Fang, J. Zhao, K.J. Yu, E. Song, A.B. Farimani, C.-H. Chiang, X. Jin, Y. Xue, D. Xu, W. Du, K.J. Seo, Y. Zhong, Z. Yang, S.M. Won, G. Fang, S.W. Choi, S. Chaudhuri, Y. Huang, M.A. Alam, J. Viventi, N.R. Aluru, J.A. Rogers, Ultrathin, transferred layers of thermally grown silicon dioxide as biofluid barriers for biointegrated flexible electronic systems, Proc. Natl. Acad. Sci. 113 (42) (2016) 11682–11687, doi:10.1073/pnas.1605269113.

[74] E. Song, J. Li, J.A. Rogers, Barrier materials for flexible bioelectronic implants with chronic stability—current approaches and future directions, APL Mater. 7 (5) (2019) 050902, doi:10.1063/1.5094415.

[75] R. Merget, T. Bauer, H. Küpper, S. Philippou, H. Bauer, R. Breitstadt, T. Bruening, Health hazards due to the inhalation of amorphous silica, Arch. Toxicol. 75 (11–12) (2001) 625–634, doi:10.1007/s002040100266.

[76] C.C. Leung, I.T.S. Yu, W. Chen, Silicosis, The Lancet 379 (9830) (2012) 2008–2018, doi:10.1016/s0140-6736(12)60235-9.

[77] R. van Dijkhuizen-Radersma, S. Hesseling, P. Kaim, K. de Groot, J. Bezemer, Biocompatibility and degradation of poly(ether–ester) microspheres: in vitro and in vivo evaluation, Biomaterials 23 (24) (2002) 4719–4729, doi:10.1016/s0142-9612(02)00220-x.

[78] R. van Dijkhuizen-Radersma, J. Roosma, P. Kaim, S. Métairie, F. Péters, J. de Wijn, P. Zijlstra, K. de Groot, J. Bezemer, Biodegradable poly(ether-ester) multiblock copolymers for controlled release applications, J. Biomed. Mater. Res. Part A 67A (4) (2003) 1294–1304, doi:10.1002/jbm.a.20044.

[79] F.J. Chaparro, K.F. Presley, M.A.C. da Silva, N. Mandan, M.L. Colachis, M. Posner, R.M. Arnold, F. Fan, C.R. Moraes, J.J. Lannutti, Sintered electrospun poly(ε-caprolactone)–poly(ethylene terephthalate) for drug delivery, J. Appl. Polym. Sci. 136 (26) (2019) 47731, doi:10.1002/app.47731.

[80] M. Sokolsky-Papkov, K. Agashi, A. Olaye, K. Shakesheff, A.J. Domb, Polymer carriers for drug delivery in tissue engineering, Adv. Drug Deliv. Rev. 59 (4–5) (2007) 187–206, doi:10.1016/j.addr.2007.04.001.

[81] K.-Y. Law, Definitions for hydrophilicity, hydrophobicity, and superhydrophobicity: getting the basics right, J. Phys. Chem. Lett. 5 (4) (2014) 686–688, doi:10.1021/jz402762h.

[82] V. Gun'ko, V. Zarko, R. Leboda, E. Chibowski, Aqueous suspension of fumed oxides: particle size distribution and zeta potential, Adv. Colloid Interface Sci. 91 (1) (2001) 1–112, doi:10.1016/s0001-8686(99)00026-3.

[83] M. Kosmulski, pH-dependent surface charging and points of zero charge. IV. update and new approach, J. Colloid Interface Sci. 337 (2) (2009) 439–448, doi:10.1016/j.jcis.2009.04.072.

[84] J.-H. Oh, C.H. Park, Robust fluorine-free superhydrophobic PET fabric using alkaline hydrolysis and thermal hydrophobic aging process, Macromol. Mater. Eng. 303 (7) (2018) 1700673, doi:10.1002/mame.201700673.

[85] A.A. Dameron, D. Seghete, B.B. Burton, S.D. Davidson, A.S. Cavanagh, J.A. Bertrand, S.M. George, Molecular layer deposition of alucone polymer films using trimethylaluminum and ethylene glycol, Chem. Mater. 20 (10) (2008) 3315–3326, doi:10.1021/cm7032977.

[86] X. Liang, A.W. Weimer, Photoactivity passivation of TiO_2 nanoparticles using molecular layer deposited (MLD) polymer films, J. Nanopart. Res. 12 (1) (2009) 135–142, doi:10.1007/s11051-009-9587-0.

[87] R.L. Patel, Y.-B. Jiang, X. Liang, Highly porous titania films coated on submicron particles with tunable thickness by molecular layer deposition in a fluidized bed reactor, Ceram. Int. 41 (2) (2015) 2240–2246, doi:10.1016/j.ceramint.2014.10.026.

[88] K. Van de Kerckhove, F. Mattelaer, D. Deduytsche, P.M. Vereecken, J. Dendooven, C. Detavernier, Molecular layer deposition of "titanicone", a titanium-based hybrid material, as an electrode for lithium-ion batteries, D top Dalton Trans. 45 (3) (2016) 1176–1184, doi:10.1039/c5dt03840e.

[89] A. Reznickova, Z. Novotna, Z. Kolska, V. Svorcik, Immobilization of silver nanoparticles on polyethylene terephthalate, Nanoscale Res. Lett. 9 (1) (2014) 305, doi:10.1186/1556-276x-9-305.

[90] T. Tkavc, I. Petrinič, T. Luxbacher, A. Vesel, T. Ristić, L.F. Zemljič, Influence of O_2 and CO_2 plasma treatment on the deposition of chitosan onto polyethylene terephthalate (PET) surfaces, Int. J. Adhes. Adhes. 48 (2014) 168–176, doi:10.1016/j.ijadhadh.2013.09.008.

[91] A. Sood, P. Sundberg, J. Malm, M. Karppinen, Layer-by-layer deposition of ti–4,4′-oxydianiline hybrid thin films, Appl. Surf. Sci. 257 (15) (2011) 6435–6439, doi:10.1016/j.apsusc.2011.02.022.

[92] P. Sundberg, M. Karppinen, Organic and inorganic–organic thin film structures by molecular layer deposition: a review, Beilstein J. Nanotechnol. 5 (2014) 1104–1136, doi:10.3762/bjnano.5.123.

[93] F. Grillo, M.T. Kreutzer, J.R. van Ommen, Modeling the precursor utilization in atomic layer deposition on nanostructured materials in fluidized bed reactors, Chem. Eng. J. 268 (2015) 384–398, doi:10.1016/j.cej.2015.01.067.

[94] J.R. van Ommen, A. Goulas, Atomic layer deposition on particulate materials, Mater. Today Chem. 14 (2019) 100183, doi:10.1016/j.mtchem.2019.08.002.